LITERATURE REVIEWS

1. Heterogeneous Catalysis

Catalysis plays a prominent role in our society. The majority of all chemicals and fuels produced in the chemical industry has been in contact with one or more catalysts. Catalysis becomes also progressively more important in environmental pollution control. It will be even more important in the future.

A heterogeneous catalytic reaction begins with adsorption of reacting gases on catalyst surface, where intramolecular bonds are broken or weakened (Niemantsverdriet, 1995). Next the adsorbed species reacts on the surface, often in several consecutive steps. Finally, products desorb from the surface into the gas phase, thereby regenerating the active sites on the surface for following catalytic cycle. Figure 1 illustrates the sequence for one of the oldest catalytic processes, the ammonia synthesis.

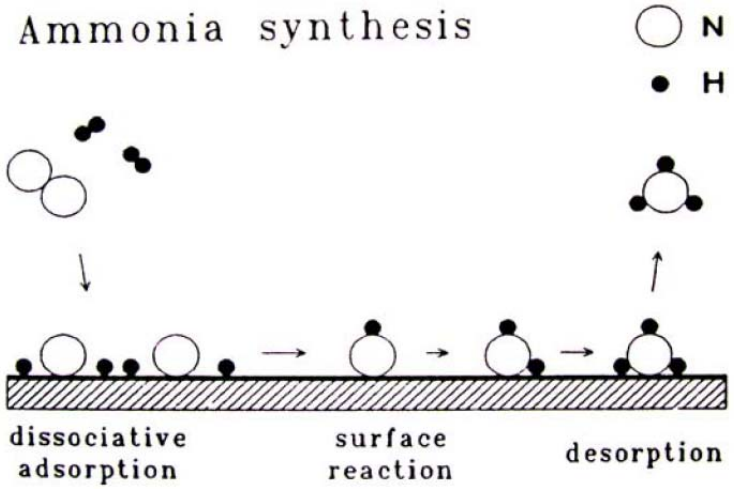

Figure 1 Schematic representation of a well known catalytic reaction, the synthesis of ammonia over iron catalysts

Source: Niemantsverdriet (1995)

As catalysis proceeds at the surface, a catalyst should preferably consist of small particles with a high fraction of surface atoms. Principal properties of a catalyst are its activity, selectivity and stability.

1.1 Perovskite Oxides

In perovskite-type oxide, represented by ABO_3, the B site cation is surrounded octahedrally by oxygen, and the A site cation is located in the cavity made by these octahedral (Figure 2). A stoichiometric ABO_3 compounds, combinations of A^{n+}, B^{m+} are given by n+m = 6, such as $CaTiO_3$, $LaMnO_3$, $LaCoO_3$ etc. The properties of perovskite-type oxides depend tightly on the nature of A and B ions and on the valence state of A and B. The A ions are in general catalytically inactive and influence thermal stability of perovskite, while the active ions in the B position are placed at such relatively large distance from each other that reactant molecule interacts only with a single site.

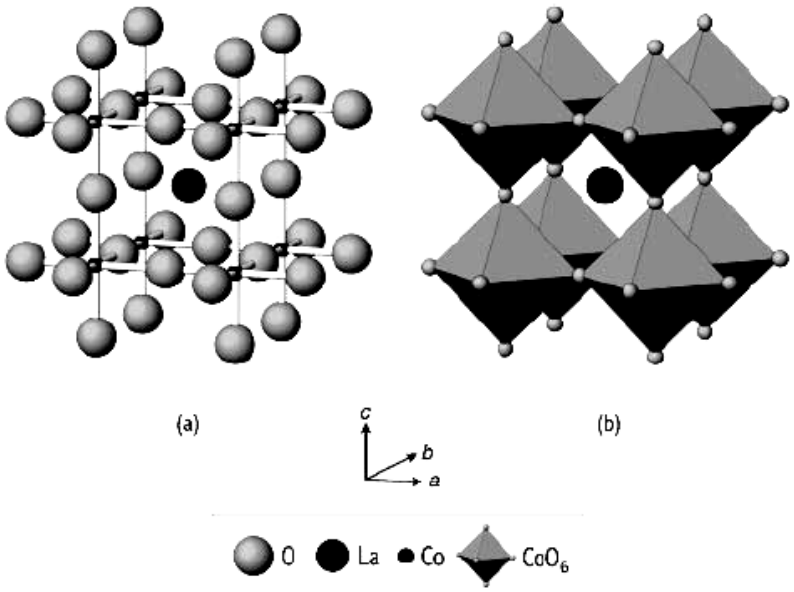

Figure 2 Crystal structure of $LaCoO_3$ showing (a) atomic positions of the unit cell and (b) structure depicting CoO_6 corner-sharing octahedra, with the A cations occupying the central interstice, and the B cations residing in the centre of the octahedra

Source: Read *et al.* (2002)

The transition metal B in perovskites can be particularly active in oxidative catalysis if it can fluctuate between two stable oxidation states (Spinicci *et al.*, 2002). By this way it is possible to balance electrically:

(1) the insertion of O^{2-} ions in the lattice from the gas-phase O_2, and the related capture of electrons ($O_2 + 4e^- \Rightarrow 2O^{2-}$);

(2) the formation of O radicals which can be bound to the hydrocarbon from lattice O^{2-} ($2O^{2-} \Rightarrow 2O + 4e^-$).

Voorhoeve (Voorhoeve, 1977) proposed two types of catalytic processes for perovskite-type catalysts: one is the suprafacial and the other the intrafacial process. The suprafacial process is the reaction on the surface. The intrafacial process, including the release of oxygen from the lattice or the reverse process, shows the redox behaviors.

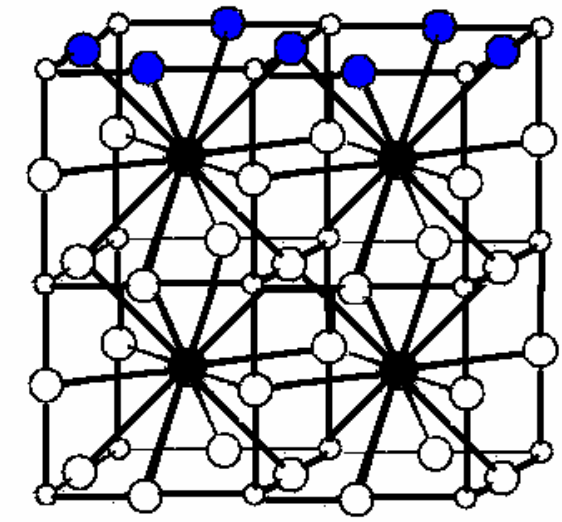

Figure 3 Two types of oxygen:

● adsorbed oxygen (α-oxygen), o lattice oxygen (β-oxygen)

Two types of oxygen are considered to participate in desorption of oxygen from the outermost layers of the perovskite structure, which form the active surface of

the material: the adsorbed oxygen (α-oxygen) and the lattice oxygen (β-oxygen) shown in Figure 3.

The first, α-oxygen, is due to oxygen adsorbed on the catalytic surface. It is accommodated in the O^{2-} vacancies formed by the partial substitution of A-site cations by lower valence ions or even by vacancies of B-site cations, and involves diffusion of O^{2-} ions through the lattice with the formation of neighboring high valence metal ions. This form is believed to be more active and reacts with hydrocarbons at lower temperatures than the β-oxygen. The mechanism of oxidation on these species is generally referred as suprafacial because it is connected with the presence of anionic vacancies on the surface. The second, β-oxygen, is observed for substituted as well unsubstituted samples. The diffusion of this type of oxygen inside the lattice is accompanied by A and/or B ions diffusion and is therefore activated at higher temperatures in respect to α-oxygen. The mechanism of oxidation on these species is generally referred as intrafacial, because connected to the presence of lattice species in the layers near to surface.

Spinicci *et al.* (2002) considered oxygen desorption from perovskite using $LaMnO_3$ as a representative catalyst by temperature programmed desorption technique (TPD). The two oxygen TPD peaks were obtained. The first one centered at low temperature about 723 K referred to adsorbed oxygen on anionic vacancies. The second one centered at high temperature about 923 K referred to lattice. These peaks corresponded to α and β-oxygen, the α-oxygen is more mobile and the β-oxygen is more strongly bound. This event was confirmed by x-ray photoemission (XPS) spectra. The XPS spectra showed asymmetrical O1s spectra (Zhang *et al*., 2005). It revealed that oxygen species exist a mix oxidation state on catalyst surface. The oxygen species were lattice oxygen species at lower binding energy and adsorbed oxygen species at higher binding energy. The relative content of two kinds of oxygen can be estimated from the relative area of sub-peaks.

The nature and reactivity of α-oxygen may be greatly different from β-oxygen which forms a rigid crystal lattice, because the α-oxygen is more weakly

bonded to metal cations than the normal β-oxygen. Such weakly bonded oxygen is considered to be effective to complete combustion (Tejuca and Fierro, 1993).

1.2 Catalyst Preparation

In general, perovskites have been prepared by calcining a solid mixture of constituent metal oxides or carbonates (the method used in the ceramic industry), or by evaporation an aqueous solution of constituent metal nitrates or acetates and by subsequent calcination. The resulting oxides have relatively small surface areas.

1.2.1 Sol – gel method

The sol – gel involves first the formation of a sol followed by that of a gel. A sol, which is liquid suspension of solid particles ranging in size from 1 nm to 1 micron, can be obtained by the hydrolysis and partial condensation of precursor such as an inorganic salt or metal alkoxide. The further condensation (polymerization) of sol particles into three-dimensional network produces a gel, which is a diphasic material with a solid encapsulating solvent. The encapsulated liquid can be removed from a gel by either evaporative drying or drying with supercritical extraction (supercritical drying for short). The resulting solid products are known as a xerogel and an aerogel, respectively.

The single most important characteristic of sol gel preparation of catalytic materials is its ease of control that translates into the following advantages:

- the ability to maintain high purity (because of purity of starting materials);
- the ability to change physical characteristics such as pore size distribution and pore volume;
- the ability to vary compositional homogeneity at molecular level;
- the ability to prepare samples at low temperatures;
- the ability to introduce several components in a single step;

- the ability to produce sample indifferent physical forms.

There are four key steps in taking a precursor to a particular product form via sol – gel preparation: formation of a gel, aging, removal of the solvent, and calcination/sintering (Figure 4). The important parameters in the various steps of a sol – gel process are shown in Table 1. The versatility of this preparative approach lies in the number of parameters that can be manipulated in each of these steps:

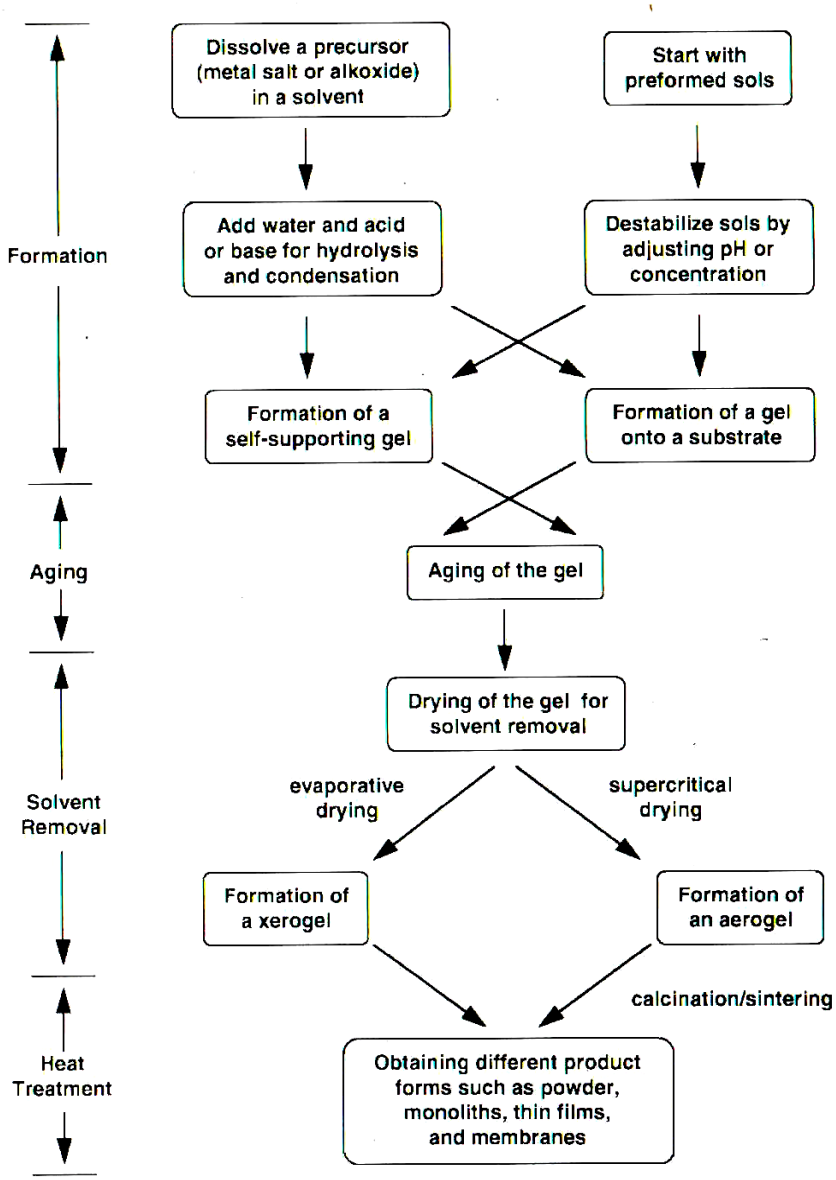

Figure 4 The various steps of a sol – gel process

Source: Ertl *et al*. (1999)

Table 1 Important parameters in various steps of sol – gel process

Step	Purpose	Important parameter
Solution chemistry	to form a gel	- type of precursor - type of solvent - pH (acid/ base content) - water content - precursor concentration - temperature
Aging	to allow a gel to undergo changes in properties	- time - temperature - composition of the pore liquid (e.g. pH) - aging environment (e.g. humidity)
Drying	to remove solvent from a gel	- drying method (e.g. evaporative, supercritical freeze drying) - temperature and heating rate - pressure and pressurization rate - time
Calcination/ sintering	to change physical/chemical properties of the solid, often resulting in crystallization and densification	- temperature and heating rate - time - gaseous environment (e.g. inert, reactive gas)

Source: Ertl *et al*. (1999)

a. Solution chemistry

A precursor in a sol – gel preparation can either be a metal salt/alkoxide dissolved in an appropriate solvent or a stable colloidal suspension of performed sols. Metal alkoxides have been the most extensively used because they are commercially available in high purity and their solution chemistry has been

documented. Sol – gel chemistry with metal alkoxides can be described in terms of two classes of reactions:

Hydrolysis:

$$–M–OR + H_2O \longrightarrow –M–OH + ROH$$

Condensation:

$$–M–OH + XO–M– \longrightarrow M–O–M + XOH$$

where X can either be H or R (an alkyl group)

A three-dimensional network comes from the condensation of partially hydrolyzed species. The hydrolysis and condensation reactions are nucleophilic displacement reactions which the reactivity of the metal alkoxide depends on the positive partial charge of the metal atom and its coordination number. A small positive partial charge and the larger bulk alkoxide group show the less reactive in hydrolysis and condensation. The amount of water and adding rate also influence gel characteristic. With the hydrolysis ratio (h), the mole of water per mole of metal alkoxide $M(OR)_m$, three specific regions can be defined as follows: (i) the hydrolysis ratio less than 1, an infinite network seldom form due to the low functionality of the precursor towards condensations. Because there are few M-OH groups for cross-linking, gelation or precipitation cannot occur when there is no local excess of water. (ii) At $1< h < m$, polymeric gel can form, and (iii) $h > m$, the cross-link polymers, particulate gels, or precipitate can form when an excess of water is added to the alkoxides. Temperature and solvent are also important factors in sol gel process. Varying the temperature is most effective when it can alter the relative rates of competing reactions. Solvent can change the nature of an alkoxide through solvent exchange or affect the condensation reaction directly.

The effect of sol - gel parameters discussed on gel properties can often be followed by an experimental observable known as gel time. At the gel point, a continuous solid phase contains a structure that reflects the formation and branching of particle under specific growth conditions. These particular phases are important

because it is the genesis of structural evolution that takes place in all subsequent processing steps.

b. Aging

Aging represents the time between the formation of a gel and removal of solvent. As long as pore liquid remains in the matrix, a gel is not static and can undergo many transformations. For alkoxide-derived gels, condensation between surface functional groups continues to occur after the gel point. This process can actually be desirable because it leads to a more cross-linked network that is mechanically stronger and easier to handle. However, extensive condensation causes the gel shrinked due to solvent being expelled, in a phenomenon called “syneresis”. The dissolution and re-precipitation of particles result an increase in the average pore size of the gel and a decrease in its specific surface area. Parameters that affect this aging process include temperature, time, and pH of the pore liquid.

c. Drying

As the pore liquid is evaporated from the gel network, the capillary pressure associated with the liquid-vapor interface within the pore can become very large for small pore. With a distribution of pore sizes in the gel, the differential pressure across pores of different sizes leads to a collapse in the pore structure. Thus, strategies those are effective in maintaining the integrity of the gel network aim at minimizing either the differential pressure or the capillary pressure itself. The easiest way to understand approaches that are effective in minimizing the capillary pressure directly is to examine the equation

$$P = 2\sigma \cos(\alpha) / r \qquad .....(1)$$

Where P is capillary pressure, σ is surface tension, α is the contact angle between liquid and solid, and r is pore radius. For a given pore size, then, the capillary pressure can be reduced by (i) using a solvent with a lower surface tension or with a

contact angle close to 90° and (ii) eliminating the liquid-vapor interface altogether with either supercritical or freeze drying.

Supercritical drying is high-pressure approach aimed at eliminating liquid-vapor interface and the accompanying capillary surface. There are now numerous examples showing that aerogel can be prepared to give high porosities, high specific surface areas, low apparent densities and good textural stability. These advantages can be realized because, in addition to eliminating the liquid-vapor interface, supercritical drying is done at moderate temperature. Similar to aging, the gel is not static during drying and, for that reason, drying can be viewed as part of the overall aging process. The properties of a product are thus dependent on the drying method and drying conditions.

d. Calcination/Sintering

After the removal of the pore liquid, further heat treatment is necessary to convert a xerogel and an aerogel into a catalytically useful form. This heating serves several purposes – it decomposes anions such as alkoxides or carbonates to give oxide, it allows rearrangement of the structure of the solid and it allows crystallization to occur. Heating is done in the presence of reactive gas (e.g. flowing air, oxygen, or hydrogen) in order to burn off any residual organics or to oxidize (or reduce) a sample. Exposing the sample to high temperature over a period of time leads to sintering and consequently a decrease in surface area. Thus, the physical characteristics of a product depend on parameters such as temperature, heating rate, time and gaseous environment.

1.2.1.1 Studied sol – gel methods

(a) The Pechini method

The Pechini method was a process related to the sol – gel route (Pechini, 1967) named after its American inventor, Maggio Pechini. This

method utilizes the ability of certain alpha-hydroxycarboxylic acids of citric acid, to form polybasic acid chelates with metal ions. The starting solution is a mixture of metallic salts and a hydroxyl acid in which a polyalcohol, most often ethylene glycol, is added to the initial solution. The polyalcohol is supposed to promote the reticulation in the transformation of the starting solution to the rigid foam. The reticulation or polymer formation is due to the esterification reaction between citric acid and the polyalcohol.

Basically, the process consists of the following three steps (Popa *et al.*, 2002):

(i) the complexation of metal ions with citric acid in water without aging and pH adjusting;

(ii) the polymerization, where the formed chelates undergo polyesterification when treated with a polyhydroxyalcohol, such as ethylene glycol, with the formation of a stable polymeric network; and

(iii) the decomposition of the formed organic network to obtain the powder precursor after boiling at moderate temperature (~ 363 K). On removal of the excess solvent by heating, no crystallization occurs, a transparent resin containing the metals in solid solution was formed. The temperature has been proved to be very important, at temperatures higher than 363 K, the solution becomes turbid in time generating nontransparent final resin, which can be explained by the formation of insoluble precipitates from the rapid hydrolysis of the metal-citrate species. At lower temperatures, a longer time is needed to obtain the stable polyester network.

This technique allows the suitability and advantages to prepare materials at low temperatures with flowing oxygen and calcining no long periods and to provide homogeneous small particle size powders with high sinterability. Numerous researchers had synthesized the perovskite via the Pechini method. Complete crystallization of powders obtained at 973 K for 4 hours for $LaCoO_3$ (Sinquin *et al.*, 2001), 6 hours for $LaFeO_{3+d}$ (Popa *et al.*, 2002), 8 hours for

$LaAlO_3$ and 6 hours for $LaMnO_{3+d}$ (Kakihana *et al.*, 1998). The mean crystallite sizes were in the nanoscale range.

The amount of citric acid used as a chelating ligand plays an important role in remaining the homogeneity of gel precursor (Kakihana *et al.*, 1999). $BaTiO_3$ prepared by the polymerizable citrate complex method indicated the formation of a mixed-metal citrate complex with stoichiometry close to Ba/Ti/citric acid = 1:1:3 using Raman and NMR spectroscopy. Both barium and titanium ions were simultaneously stabilized with citric acid. While Fernandes *et al.* (2002) prepared $LaNiO_3$ with mole ratio of citric acid to ethylene glycol being 3:2. The XRD patterns were obtained only from the product calcined at 1073 K clearly suggesting the formation of a highly crystallized perovskite.

(b) Schiff base complex method

A Schiff base derived from an amine and an aldehyde is an important ligand that coordinates to metal ions via azomethine nitrogen (C=N). Schiff base complexes are important for designing metal complexes related to synthetic and natural oxygen carriers (Canplot *et al*., 2005). Schiff bases have played an important role in the development of coordination chemistry as they readily form stable complexes with most of the transition metals. The complexes make the compounds effective and stereospecific catalysts for oxidation, reduction and transformations of organic and inorganic chemistry.

A Schiff base ligand represents one of the most widely utilized classes of ligands in metal coordination chemistry. Synthesis of tetradentate Schiff base ligands by reaction between diamines and a corresponding salicylaldehyde derivative is an important reaction in organic chemistry due to the great number of molecules that can be generated and the well-known ability of these tetradentate ligands to form stable complexes with different metal cations (Revenga-Parra *et al*., 2005).

The first salen – type [salen = N,N-bis(salicylidene) ethane-1,2-diamine] Schiff base metal complexes were synthesized in 1933 by condensing salicylaldehyde and ethylenediamine with various metal salts by a one – pot method (Haikarainen, 2005). Most of the products were brightly colored solids, with the color dependent on the metal. Later it became customary first to prepare the organic salen ligand and then to complex it with the desired metal salt. The standard method for the preparation of the ligand has been and still is the condensation of salicylaldehyde or its derivative with ethylenediamine or its derivative in alcohol solvent, usually ethanol or methanol (Figure 5).

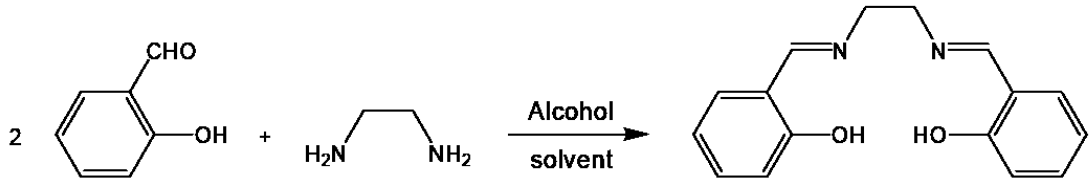

Figure 5 Synthesis of basic salen structure
Source: Haikarainen (2005)

Salen ligands are prepared by the condensation of two equivalents of a salicylaldehyde derivative with a 1,2-diamine, and the simplest, achiral version is prepared from salicylaldehyde and ethylenediamine. This tetradentate bis(imine) ligand are accessed simply by using chiral 1,2-diamines. Metal complexes of salen ligands are readily prepared from a variety of first row and second row transition metal salts as well as main group metals. The appropriate metal for the desired reactivity has been identified, the modularity of synthesis of salen ligands allows for the systematic tuning of catalyst steric and electronic properties by modification of the metal counterion, the chiral diamine or the salicylaldehyde components. Although a large number of ligand structures are thus accessible, it is striking that 1,2-diamines salen ligand has often been found to be the optimum ligand for a broad range of reactions catalyzed by several different metals.

Pui *et al*. (2001) studied the synthesis and characterization of some new cobalt(II) complexes with tetradentate Schiff bases derived from bis(salicylaldehyde)ethylenediimine. The Schiff bases-type ligands

employed have been obtained by refluxing an aldehyde with a corresponding diamine (2:1 molar ratio). The synthesis of coordinative compounds involves the refluxing of an alcoholic solution of ligands in the form of a potassium salt, with an aqueous solution of $Co(Acetate)_2 \cdot 6H_2O$. Analytical results indicated a good purity of the coordinative compounds confirmed by thermal analysis and IR spectroscopy. A comparative study of the IR spectra between the free ligands and metallic complexes, evinces modifications of the vibration bands characteristic of the azomethine group (C=N) and shifting skeletal vibration of the aromatic rings. Over the 400–700 cm^{-1}, the appearance of some new bands, characteristic to the Co–O bonding vibration, was observed.

Nathan *et al*. (2003) synthesized Cu(II) Schiff base complexes by a standard method in which two equivalents of salicylaldehyde and one equivalent of the ethylenediamine are refluxed for 1 – 1.5 hours in ethanol. Then metal Cu(II)acetate solution was mixed and refluxed for 15 – 30 minutues. The product was characterized using x-ray crystallography found that Cu(II) Schiff base complex stacked dimer with the primary ligand in a cis-planar geometry.

Developments concerning new methods, especially solution techniques involving improvement of synthesis conditions for obtaining pure phases, have been applied to lower the reaction temperature and to prepare finer and homogeneous powders.

1.2.2 Coprecipitation

The most common method for mixed – oxide catalyst preparation is crystallization or precipitation or coprecipitation in solution of a precursor form (hydroxide, oxide, insoluble salt).

Precipitation involves two main steps: nucleation and growth. At the nucleation stage, the first minute crystals of the solid phase are formed; these have a high specific surface area and high surface energy, and hence are unstable. Below a

certain critical nuclei size, the free energy of formation of the solid phase is less than its surface energy and the new phase is thermodynamically unstable. Above this critical size, the solid particles can grow.

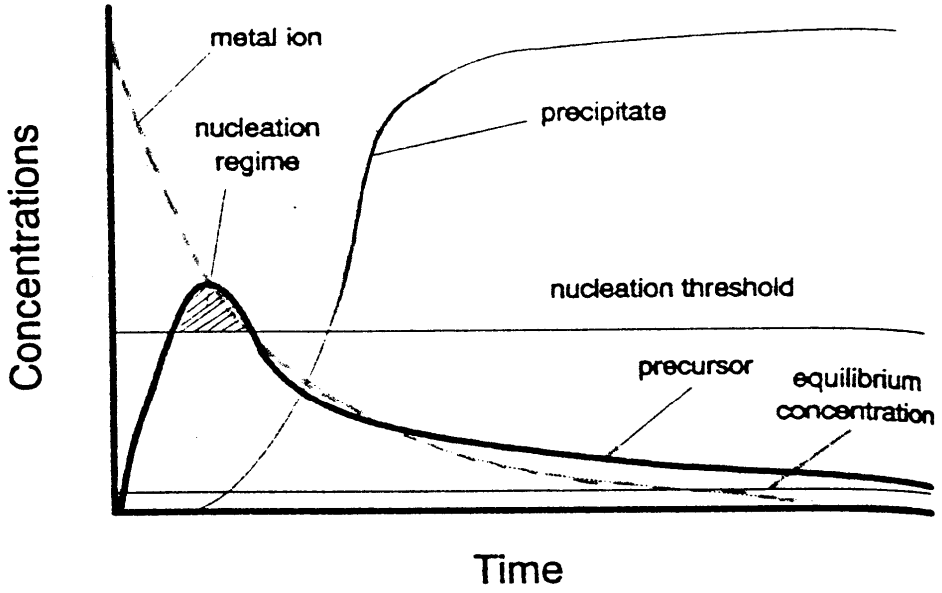

Figure 6 Simplified scheme for the formation of a solid product from solution
Source: Ertl *et al*. (1999)

The general process of the formation of a solid from a solution can be described in a simplified form as the nucleation curve which describes the development of precursor concentration with time (Figure 6). Such a precursor could, for instance, be hydrolysis product of the metal ions in solution. Only if the precursor concentration exceeds a critical threshold concentration will a nucleus form, and the precipitation begins. The nucleus is defined as the smallest solid – phase aggregated of atoms, molecules or ions which are formed during precipitation which is capable of spontaneous growth. As long as the concentration of precursor species stays above the nucleation threshold, new particles are formed. As soon as the concentration falls below the critical concentration due to consumption of precursors by nucleation or by the growth process, only particle growth of existing particles prevails. The size of the particles finally resulting from a precipitation process will be dependent on the area of the shaded section between the nucleation curve and the nucleation threshold. The

larger the area, the more particles nucleate and the smaller the resulting particles form.

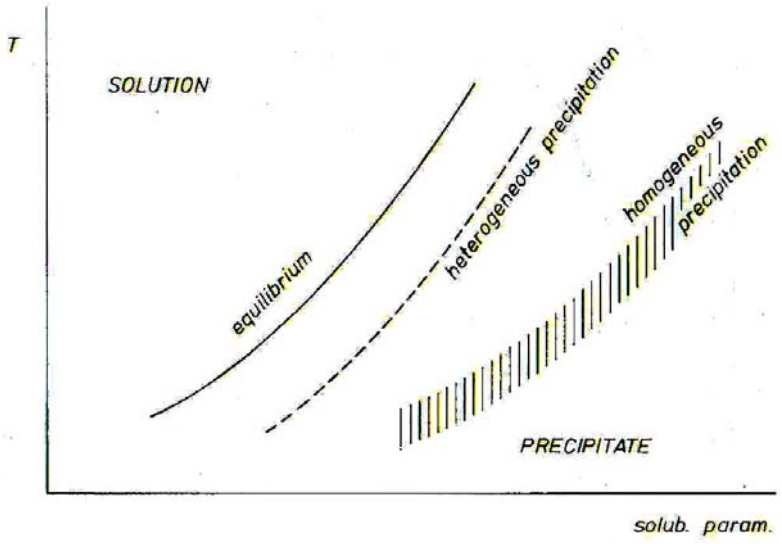

Figure 7 The precipitation conditions for a given compound
Source: Ertl *et al*. (1999)

Figure 7 represents a kind of phase diagram with two intensive parameters: temperature T and any parameter (indicated as solub. param.) on which the solubility or dissociation constant depends. This could be the pH or the concentration of a reactant or a precipitating agent. The line label equilibrium corresponds to the exact equilibrium curve separating the monophasic domain (upper left) from the biphasic domain (lower right). The new phase is not formed for a small supersaturation unless a patch of surface of that phase is already formed. In absence of any solid surface, precipitation will only occur in supersaturation conditions represent by the curve homogeneous precipitation. The upper left hand border of this band corresponds to critical nucleation conditions, namely those below which no nucleation occurs. The dotted curve represents the conditions where precipitation can occur when foreign surface is present, i.e. heterogeneous precipitation.

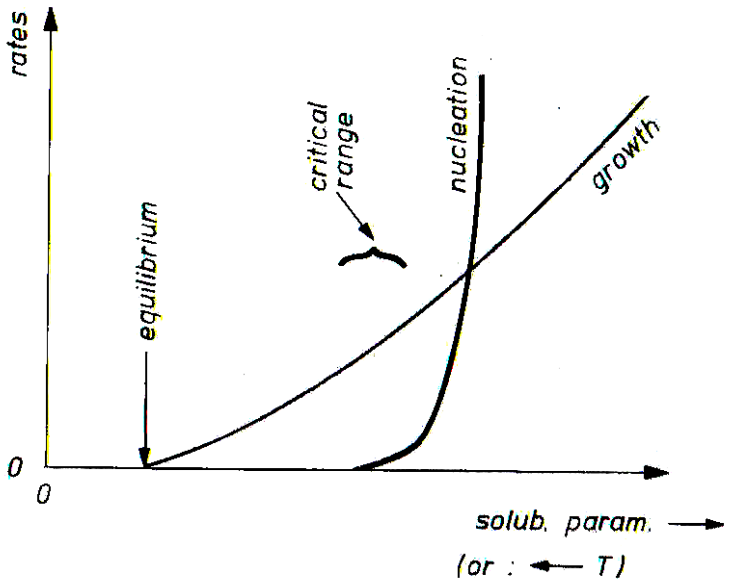

Figure 8 Qualitative comparison of the dependency of the rates of nucleation and growth of precipitate particle as a function of the solubility parameter (increasing from left to right) or T (opposite direction)

Source: Ertl *et al*. (1999)

The homogeneity is possible to increase by taking advantage of the difference of the form of nucleation and growth of precipitated crystallites. On the right of Figure 8, the rate of nucleation will be very high in comparison to growth, and very tiny particles will be obtained. On the left of Figure 8, corresponds to large particles below the critical limit for nucleation. At very high supersaturations of all compounds present in a solution, finely interdispersed particles will be formed.

According to the conditions, this growth step is mainly controlled by interface or diffusion phenomena. The first case generally corresponds to the formation of complicated solid structures. The second is more common in the precipitation processes used in catalyst preparation. Only more general statements can be given.

For nucleation:

- the higher the supersaturation, the higher will be the nucleation rate;

- any interface may play the role of a heterogeneous nucleus by lowering the surface free – energy of the new phase, and thus increase the rate of nucleation;

- in general, higher temperatures lower the nucleation rate by increasing the critical size of the nuclei – upper left boundary of the homogeneous nucleation band reflects this trend.

All this has been represented schematically in Figure 7.

For growth:

- the higher the supersaturation, the higher will be the growth rate, but it is rapidly limited by diffusion processes;

- since an increase of temperature enhances the diffusion rates, the higher will be the growth rate of the new phase.

Combining above (Figure 8), some general rules for obtaining a fine precipitate can be formulated:

- A vigorous stirring of the solution while adding the precipitant is beneficial in two ways: first, each elementary volume of solution reaches rapidly the highest degree of supersaturation; second, it comes into contact several times with the agitator and the walls of vessel, thereby promoting heterogeneous nucleation also.

- A rapid addition of the precipitating agent ensures a rapid reaching of the highest degree of supersaturation in the whole volume of the solution, hence a maximum nucleation rate is obtained. For the same reason, the best precipitating agent is the one giving the precipitate with the lowest solubility product.

- Although the situation may be very different from case to case, precipitation is often advantageously made at the lowest practical temperature, as this often favors nucleation over growth.

2. Catalyst Characterization

Catalytic properties of a surface are determined by its composition and structure on the atomic scale. Thus, the ultimate goal of catalyst characterization should be to look at the surface atom by atom, and under reaction conditions. The well defined surfaces of single crystals offer the best perspectives of atom by atom characterization, although occasionally atomic scale information can be obtained from real catalysts under *in situ* conditions as well.

2.1 Thermogravimetric analysis (TGA) (Skoog, 2000)

In a thermogravimetric analysis the mass of sample in a controlled atmosphere e.g. with O_2 or N_2, that may be possible to encourage or suppress oxidation reaction, thus controlling to some extent the nature of the thermal events occurring, is recorded continuously as a function of temperature or time as the temperature of the sample is increased (usually linearly with time). A plot of mass or mass percent as a function of time is called a thermogram, or a thermal decomposition curve.

Thermal decomposition of a sample is studied by thermal gravimetric analysis. There are three major weight loss steps. First, between room temperature to about 473 K corresponded to the evaporation of the volatile organic compounds. Second, the drastic change of weigh around 473 – 673 K was due to the decomposition of organic matter. The last weight loss, after an abrupt weight loss around 673 K, the residual organics (most probably were carbonates) that were involved in the intermediate product decomposed to obtain the desired oxide. $LaNiO_3$ (Fernandes *et al.*, 2002), $LaAlO_3$ (Kakihana, 1998) and $LaFeO_{3+d}$ (Popa, 2002) stabilized at 933 K, 1023 K and 1173 K, respectively.

2.2 Fourier Transform Infrared Spectroscopy (FTIR) (Niemantsverdriet, 1995)

Infrared spectroscopy can be considered as the first and the most important of the modern spectroscopic techniques that has found general acceptance in catalysis. The most common application of infrared spectroscopy in catalysis to identify adsorbed species and to study the way in which these species are chemisorbed on the surface of the catalyst. In addition, the technique is useful in identifying phases that are present in precursor stages of the catalyst during its preparation. The infrared spectra of adsorbed probe molecules such as CO and NO give valuable information on the adsorption sites that are present on a catalyst. The vibration is excited by the interaction of the bond with a wave field, as with photons and electrons, the excitation is subject to strict selection rules. Collisions, on the other hand, excite all vibrational modes.

Theory of Molecular Vibrations

Molecules possess discrete levels of rotational and vibrational energy. Transitions between vibrational levels occur by absorption of photons with frequencies ν in the mid-infrared range (Table 2). For small deviations of the constituent atoms from their equilibrium positions, the potential energy V(r) can be approximated by that of the harmonic oscillator:

$$V(r) = \frac{1}{2}k\left(r - r_{eq}\right)^2 \qquad \text{.....(2)}$$

where V(r) is the interatomic potential

r is the distance between the vibrating atoms

r_{eq} is the equilibrium distance between the atoms

k is the force constant of the vibrating bond.

Table 2 Classification of infrared radiation

Region	Wavelength (μm)	Energy (meV)[(a)]	Wavenumber (cm^{-1})	Detection of
Infrared	1000 – 1	1.2 – 1240	10 – 10000	Lattice vibrations
Far	1000 – 50	1.2 – 25	10 – 200	Molecular
Mid	50 – 2.5	25 – 496	200 – 4000	vibrations
Near	2.5 – 1	496 – 1240	4000 – 10000	Overtones

[(a)] 1 meV = 8.0655 cm^{-1}

Source: Niemantsverdriet (1995)

The corresponding vibrational energy levels are equidistant:

$$E_n = \left(n + \frac{1}{2}\right)h\nu \qquad \text{.....(3)}$$

$$\nu = \frac{1}{2\pi}\sqrt{\frac{k}{\mu}} \qquad \text{.....(4)}$$

$$\mu = \frac{m_1 m_2}{m_1 + m_2} \qquad \text{.....(5)}$$

where E_n is energy of the n^{th} vibrational level

n is an integer

h is the Planck's constant

ν is frequency of vibration

k is force constant of bond

μ is reduced mass

m_i is mass of vibrating atoms.

Thus, vibrational frequencies increase with increasing bond strength and decreasing mass of the vibrating atoms.

Allowed transitions in the harmonic approximation are those for which the vibrational quantum number changes by one unit. Overtones, i.e. absorption of light at a whole number of times the fundamental frequency, would not be possible. A general selection rule for the absorption of a photon is that the dipole moment of the molecule must change during the vibration. The simple harmonic oscillator of a vibrating molecule has important implications. Knowing the frequency, one can immediately calculate the force constant of the bond.

A molecule consisting of N atoms has 3N degrees of freedom. Three of these are translational degrees of freedom of the molecule and three are rotations of the molecule along the three principle axes of inertia. Linear molecules have only two rotational degrees of freedom, as no energy change is involved in the rotation along the main axis. Thus, the number of fundamental vibrations is 3N – 6 for non-linear and 3N – 5 for a linear molecules. But not all vibration can be observed. Absorption of an infrared photon occurs only if a dipole moment changes during the vibration. It is not necessary that the molecule possesses a permanent dipole, it is sufficient if a dipole moment changes during vibration.

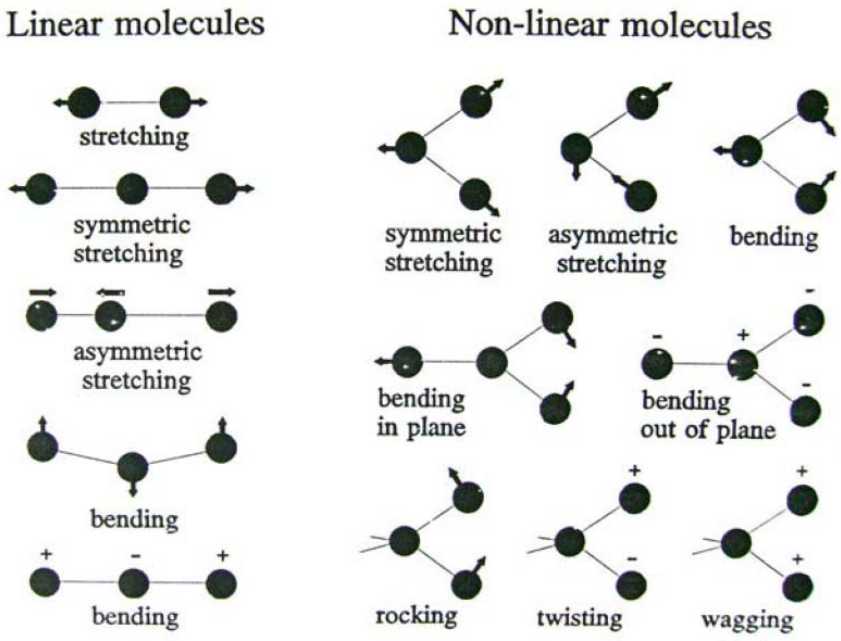

Figure 9 Fundamental vibrations of several molecules

Source: Niemantsverdriet (1995)

The group frequency concept states that functional groups in molecules may be treated as independent oscillators, irrespective of the larger structure to which they belong. As a consequence, infrared frequencies are characteristic for certain bonds in molecules and can also be used to identify species on surfaces. The following classification of characteristic stretching frequencies is a good starting point for interpreting vibrational spectra.

Transmission infrared spectroscopy is an important tool in catalyst preparation to study the decomposition of infrared active catalyst precursors as a result of drying, calcination or reduction procedures.

2.2.1 Fourier Transform Infrared Spectrometer

The early-stage IR spectrometer is of the dispersive type, which uses a prism or a grating monochromator. The dispersive spectrometer is characteristic of a slow scanning. Fourier Transform Infrared (FTIR) spectrometer obtains infrared spectra by first collecting an interferogram of a sample signal with an interferometer, which measures all of infrared frequencies simultaneously. FTIR spectrometer acquires and digitizes the interferogram, performs the Fourier Transform (FT) function, and outputs the spectrum (Figure 10).

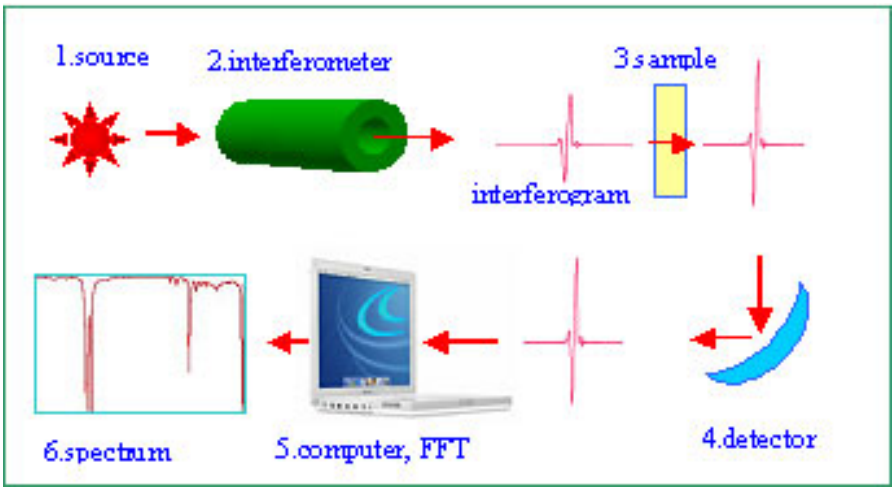

Figure 10 Schematic of an FTIR system

Source: Keck-II (2006)

FTIR spectrometer is typically based on a Michelson Interferometer shown in Figure 11. The interferometer consists of a beam splitter, a fixed mirror, and a mirror that translates back and forth, very precisely. The beam splitter is made of a special material that transmits half of the radiation striking it and reflects the other half. Radiation from the source strikes the beam splitter and separates into two beams. One beam is transmitted through the beam splitter to the fixed mirror and the second is reflected off the beam splitter to the moving mirror. The fixed and moving mirrors reflect the radiation back to the beamsplitter. Again, half of this reflected radiation is transmitted and half is reflected at the beam splitter, resulting in one beam passing to the detector and the second back to the source.

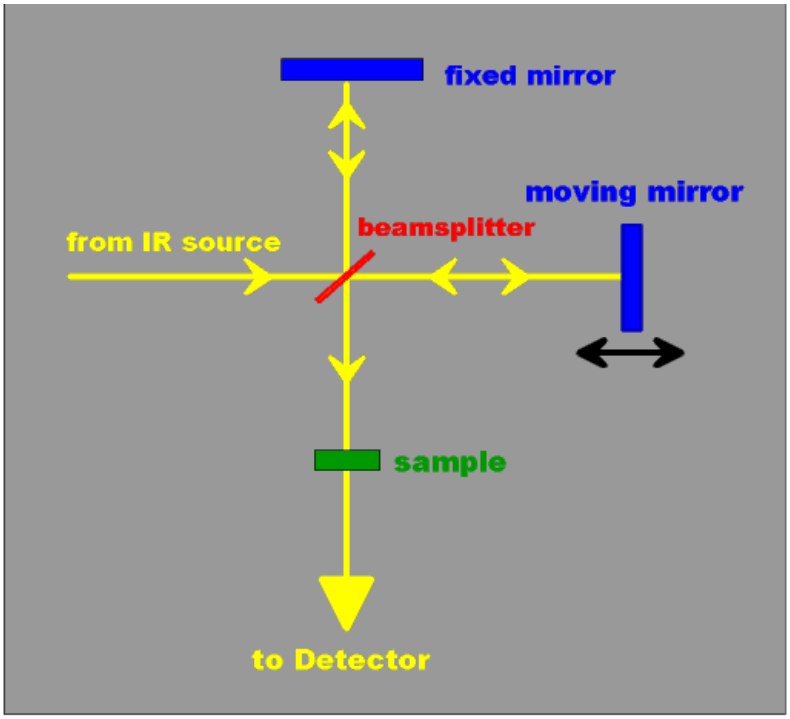

Figure 11 Schematic of a Michelson interferometer
Source: Biophysics Group (2006)

An interferometer utilizes a beamsplitter to split the incoming infrared beam into two optical beams. One beam reflects off of a flat mirror which is fixed in place. Another beam reflects off of a flat mirror which travels a very short distance (typically a few millimeters) away from the beamsplitter. The two beams reflect off of their respective mirrors and are recombined when they meet together at

the beamsplitter. The re-combined signal results from the interfering with each other. Consequently, the resulting signal is called interferogram, which has every infrared frequency encoded into it. When the interferogram signal is transmitted through or reflected off of the sample surface, the specific frequencies of energy are adsorbed by the sample due to the excited vibration of function groups in molecules. The infrared signal after interaction with the sample is uniquely characteristic of the sample. The beam finally arrives at the detector and is measure by the detector. The detected interferogram can not be directly interpreted. It has to be decoded with a well-known mathematical technique in term of fourier transformation. The computer can perform the fourier transformation calculation and present an infrared spectrum, which plots absorbance (or transmittance) versus wavenumber.

As the optical path difference, OPD, grows, different wavelengths produce peak readings at different positions and, for a broadband signal, they never again reach their peaks at the same time. Thus, as you move away from centerburst, the interferogram becomes a complex looking oscillatory signal with decreasing amplitude.

Optical Path Difference (OPD) is the optical path difference between the beams traveling through the two arms of an interferometer. OPD is equal to the product of the physical distance traveled by the moving mirror and n, the index of refraction of the medium filling the interferometer arms (air, nitrogen for purged systems, etc.).

The raw FTIR data consists of a number of (signal, OPD) pairs of values. FTIR has a natural reference point when the moving and fixed mirrors are the same distance from the beam splitter. This condition is called zero path difference or ZPD. The moving mirror displacement, Δ, is measured from the ZPD. In Figure 12 the beam reflected from the moving mirror travels 2Δ further than the beam reflected from the fixed mirror. The relationship between optical path difference, and mirror displacement, Δ, is:

$$OPD = 2\Delta \qquad \text{.....(6)}$$

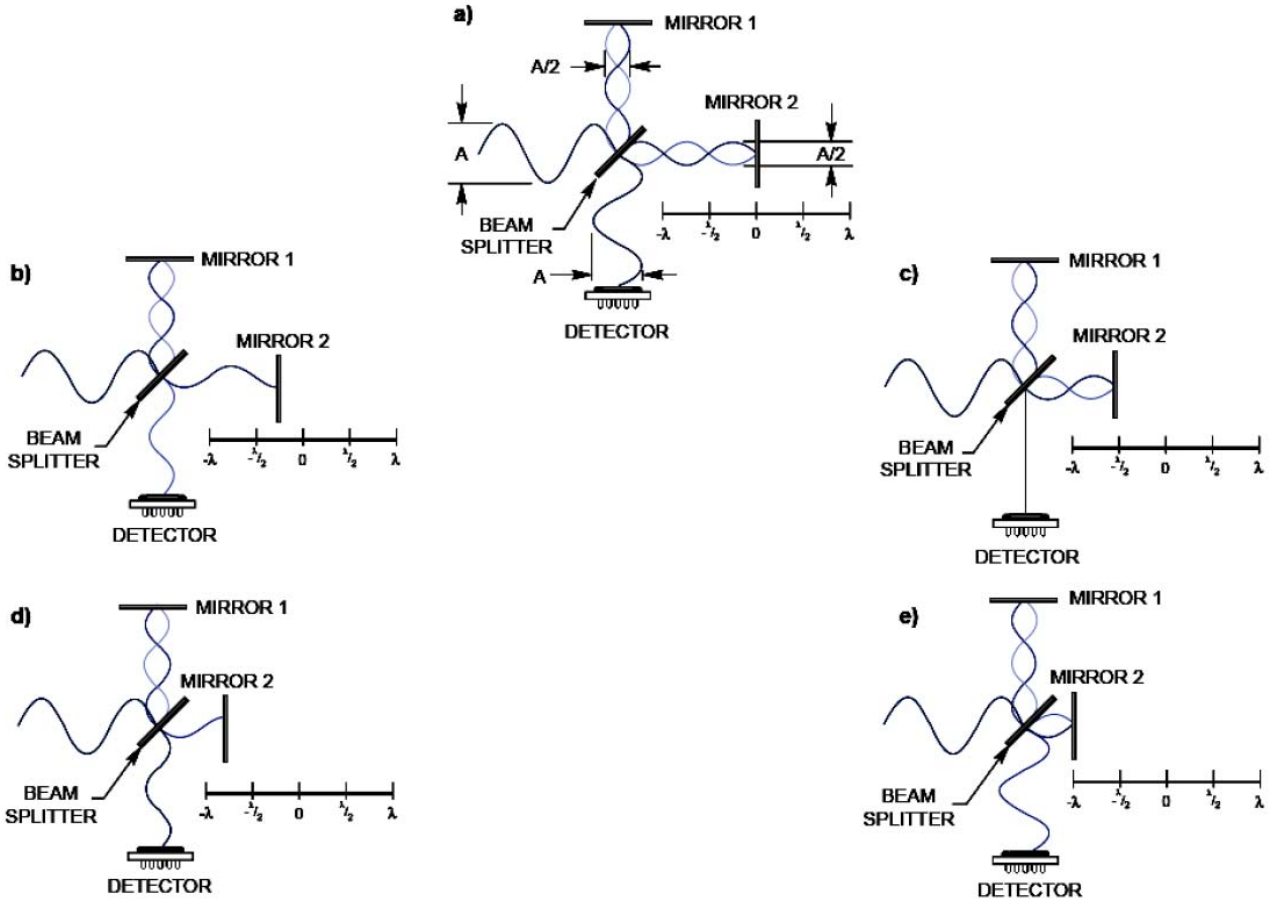

Figure 12 Schematic representation of waves and their phases, input, output, and the two arms of the interferometer as the scan goes from zero path difference condition to OPD=λ. (a) OPD=0. (b) λ/4 OPD. (c) λ/2 OPD. (d) 3λ/4 OPD. (e) 1λ OPD

Source: Anonymous (n.d.)

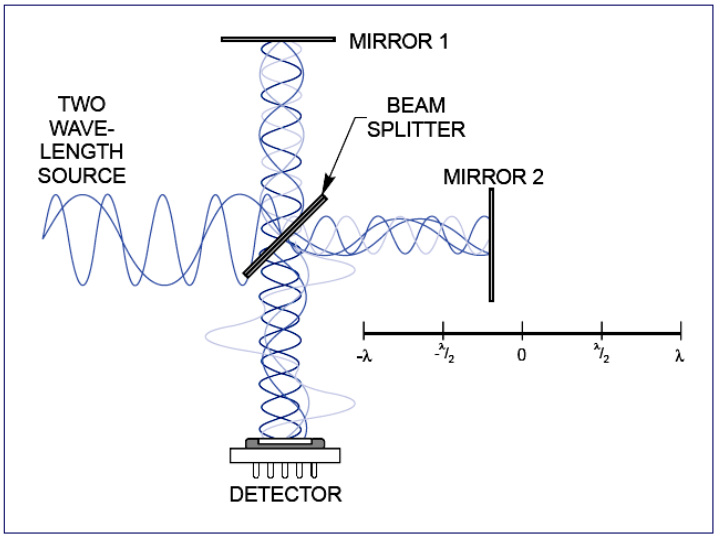

Figure 13 Two wavelength source case

Source: Anonymous (n.d.)

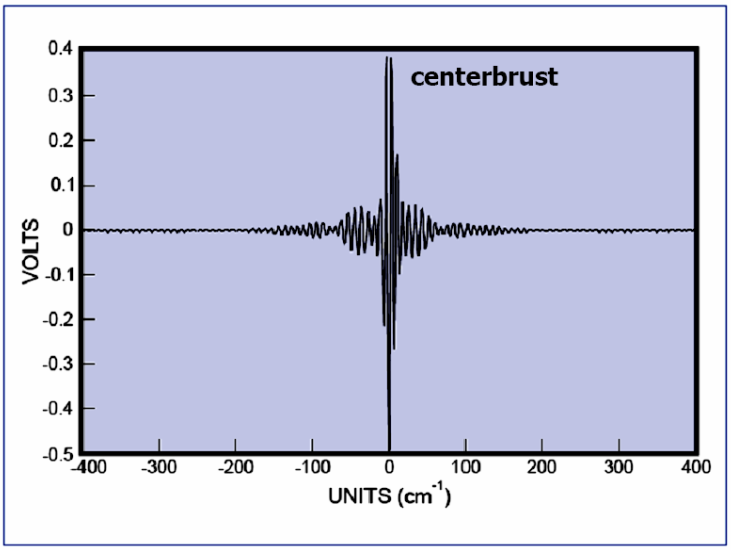

Figure 14 Interferogram

Source: Anonymous (n.d.)

Interferogram is the name of the signal format acquired by an FTIR spectrometer. It is usually significantly more complex looking than a single sinusoid, which would be expected if only a single wavelength of light was present. Figure 13 shows the beam path of a two wavelength source; Figure 14 is the interferogram of a broadband light source. The centerburst, the big spike in the center of Figure 14 is a

telltale signature of a broadband source. Its origin lies in the fact that all wavelengths are in-phase at the ZPD. Therefore, their contributions are all at maximum and a very strong signal is produced by the system of detector.

When an interferogram is fourier transformed, a single beam spectrum is generated. A single beam spectrum is a plot of raw detector response versus wavenumber. A single beam spectrum obtained without a sample is called a background spectrum, which is induced by the instrument and the environments. Characteristic bands around 3500 cm^{-1} and 1630 cm^{-1} are ascribed to atmospheric water vapor and the bands at 2350 cm^{-1} and 667 cm^{-1} are attributed to carbon dioxide. A background spectrum must always be run when analyzing samples by FTIR. When an interferogram is measured with a sample and Fourier transformed, a sample single beam spectrum is obtained. It looks similar to the background spectrum except that the sample peaks are superimposed upon the instrumental and atmospheric contributions to the spectrum. To eliminate these contributions, the sample single beam spectrum must be normalized against the background spectrum. Consequently, a transmittance spectrum is obtained as follows:

$$\%T = I/I_o \qquad \text{.....(7)}$$

Where %T is transmittance; I is the intensity measured with a sample in the beam (from the sample single beam spectrum); I_o is the intensity measured from the back ground spectrum

The absorbance spectrum can be calculated from the transmittance spectrum using the following equation:

$$A = -\log_{10} T \qquad \text{.....(8)}$$

Where A is the absorbance.

The final transmittance or absorbance spectrum should be devoid of all instrumental and environmental contributions, and only present the features of the sample. If the concentrations of gases such as water vapor and carbon dioxide in the instrument are the same when the background and sample spectra are obtained, their contributions to the spectrum will ratio out exactly and their bands will not occur. If the concentrations of these gases are different when the background and sample spectra are obtained, their bands will appear in the sample spectrum.

Some of the major advantages of FTIR over the dispersive technique include:

- Speed: Because all of the frequencies are measured simultaneously, most measurements by FT-IR are made in a matter of seconds rather than several minutes. This is sometimes referred to as the Felgett Advantage.
- Sensitivity: Sensitivity is dramatically improved with FT-IR for many reasons. The detectors employed are much more sensitive, the optical throughput is much higher (referred to as the Jacquinot Advantage) which results in much lower noise levels, and the fast scans enable the coaddition of several scans in order to reduce the random measurement noise to any desired level (referred to as signal averaging).
- Mechanical Simplicity: The moving mirror in the interferometer is the only continuously moving part in the instrument. Thus, there is very little possibility of mechanical breakdown.
- Internally Calibrated: These instruments employ a He-Ne laser as an internal wavelength calibration standard (referred to as the Connes Advantage). These instruments are self-calibrating and never need to be calibrated by the user.

The gel formation had been investigated by several researchers. Polycrystalline $La_{0.67}Sr_{0.33}MnO_3$ nano sized powders are obtained by the polymerization of citric acid and ethylene glycol (Yang *et al.*, 2005). $La_{0.67}Sr_{0.33}MnO_3$ precursor was investigated functional group using FTIR. FTIR spectra showed sharp absorption bands appeared at 1725 and 1190 cm^{-1} which could

be attributed to the monodentate ligand of metal ion with carbonyl group (COO^-). The absorption bands appeared at 1380 and 1600 cm^{-1} which were due to symmetric and asymmetric vibration of the carbonyl group. Furthermore, a strong absorption band appeared at 1180 cm^{-1}, attributed to the C–O structure from ethylene glycol in the polymerization process. The resin calcined at 823 K exhibited a pure phase of perovskite.

Nishizawa *et al.* (1997) synthesized $BaTiO_3$ by heating the mixed solution of monohydrated barium hydroxide and titanium isopropoxide in ethylene glycol. FTIR analysis was performed whereby the gel was heated in a furnace at several temperatures up to 973 K. Neat ethylene glycol is characterized by two absorption bands, due to the C–O stretching at 1086 and 1043 cm^{-1}. The disappearance of these ethylene glycol bands proved that H–O–C bonds have been replaced by Ti–O–C bonds assigned to ethylene glycoxy groups linked to titanium. At 673 K, the bands due to ethylene glycol completely disappeared and the bands related to carbonate formation appeared.

Reaction between 5,5'-methylene bis(salicylaldehyde) and 1,2-diaminoethane in equimolar ratio leaded to the formation of new polymeric chelating ligands abbreviated herein as $[–CH_2H_2(salen)–]_n$ (Maurya *et al.*, 2003). These ligands reacted with acetates of copper(II), nickel(II) and cobalt(II) to give coordination polymers. From IR spectra, ligand exhibited C=N stretching at 1633 cm^{-1}. A significant shift of this band indicated the coordination of azomethine nitrogen to the metal ions.

Kaczmarek *et al.* (2004) investigated the lanthanide salicylaldimines. The complexes were prepared in ethanol through one-step template reaction of salicylaldehyde with 4-methyl-1,3-phenylenediamine in the presence of lanthanum(III) nitrate. The IR spectra of the complexes showed a significant decrease in the C–O stretching frequency compared to the free ligand. A parallel shift of the C=N stretching mode toward higher wavelengths indicated the coordination of the

oxygen atoms of unionized OH groups, which reduced the strengthening of the hydrogen bonds between the O–H and C=N groups.

$LaCoO_3$ powders were prepared using the polymerized complex technique at relatively low temperature (Khali, 2003). The IR spectrum revealed that the major bands at 1460 cm^{-1} related to the decomposition or oxidation of the carboxylate and ester groups. These bands decreased in intensity by increasing the heating temperature and disappeared at temperatures higher than 823 K in static air. A broad feature around 600 cm^{-1} related to the formed metal-oxygen stretching appeared and sharpened at higher sintering temperature. When $LaCoO_3$ precursor was calcined at 1073 K, the spectra absorption band due to Co–O stretching appeared at 596 and 552 cm^{-1}.

2.3 X-ray method

X-rays have wavelengths in the angstrom range, are sufficiently to penetrate solid and are well suited to probe their internal structure. X-ray techniques were used to obtain much information on the physico chemical properties, such as x-ray diffraction spectroscopy (XRD), x-ray photoelectron spectroscopy (XPS) and x-ray fluorescence spectroscopy (XRF).

Incident particle knocks electrons out of the occupied states around the atom leaving empty states (vacancies) [Figure 15(a)]. Then, electron in occupied state makes transition to unfilled vacancy. X-ray is emitted to conserve energy [Figure 15(b)].

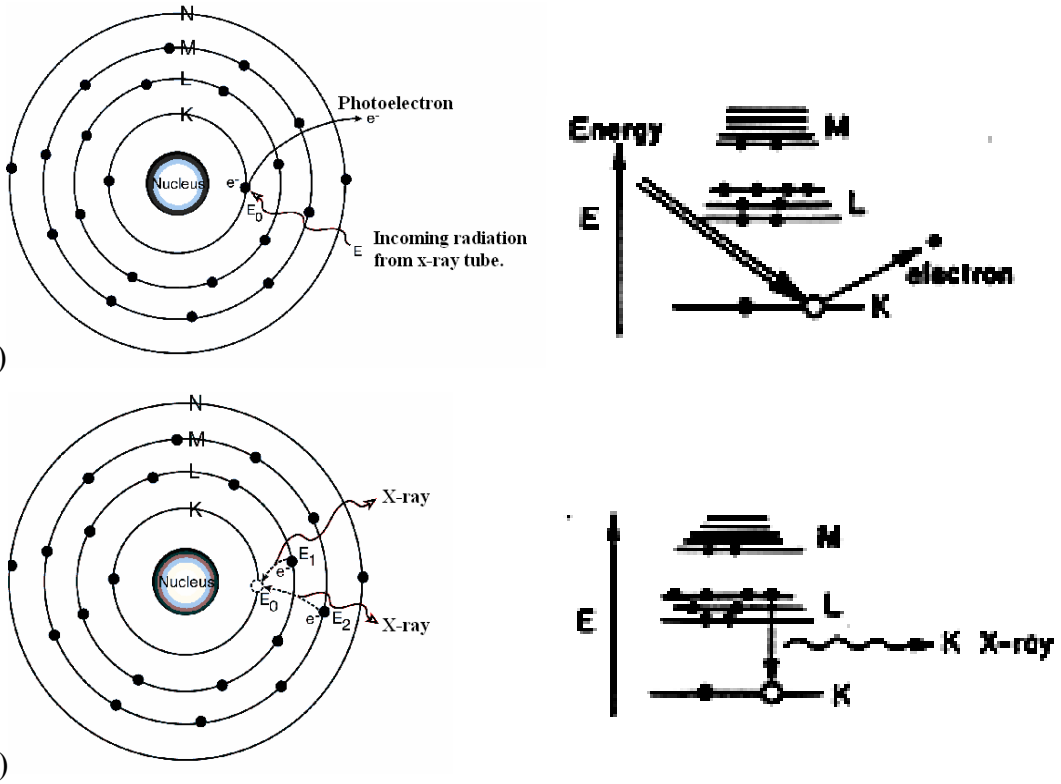

Figure 15 (a) an electron is ejected from ground state,
(b) other electron from one of the upper levels falls to ground state

2.3.1 Powder X-ray Diffraction (XRD) (Niemantsverdriet, 1995)

X-rays diffraction spectroscopy is a well-known and most frequently applied technique in catalyst characterization. This technique is a versatile, nondestructive analytical technique for identification and quantitative determination of the various crystalline forms, known as phase, of compound present in powder and solid samples. Identification is achieved by comparing x-ray diffraction pattern (diffractogram) obtained from an unknown sample with an internationally recognized database containing reference patterns. A crystal lattice is a regular three dimensional distribution, cubic, fluorite, etc, of atom in space. These are arranged so that they form a series of parallel planes separated from one another by a distance d, which varies according to the nature of the material. For any crystal, plane exits in a number of different orientations, each with its own specific d-spacing. X-ray diffraction is the elastic scattering of x-ray photons by atom in a periodic lattice. The scattered

monochromatic x-rays that are in phase give constructive interference. Figure 16 illustrates how diffraction of x-rays by crystal planes allows one to derive lattice spacing by using the Bragg's equation:

$$n\lambda = 2d\sin\theta \qquad \text{.....(9)}$$

where λ is the wavelength of the x-rays

d is the distance between two lattice planes

θ is the angle between the incoming x-rays and the normal to the reflecting lattice plane

n is the integer called of the reflection.

The primary use of the Bragg's law is in the determination of the spacing (d) between two planes (h k l) in the lattice.

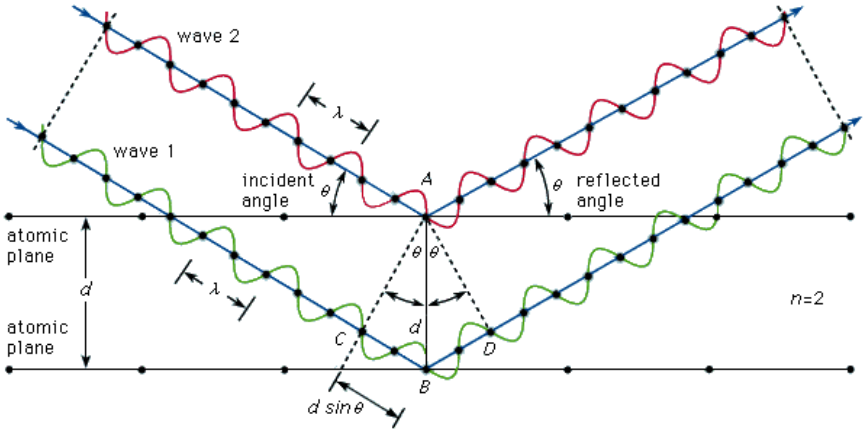

Figure 16 Bragg diffraction

Source: Britannica (1997)

A monochromatic x-ray beam with wave length λ incident on lattice plane in a crystal at an angle (θ), diffracts only when the distance traveled by the rays reflected from successive planes differs by a complete number n of wavelengths. By varying the angle (θ), the Bragg's law conditions are satisfied by different d-spacing in crystalline materials. By plotting the angular positions and intensities of the resultant diffraction peaks produce a pattern which is characteristic of the sample.

Where a mixture of different phase is present, the diffractogram is formed by addition of the individual pattern. The d-spacing of set of planes as the perpendicular distance between any pair of adjacent planes is correlated with unit cell parameters shown in Table 3.

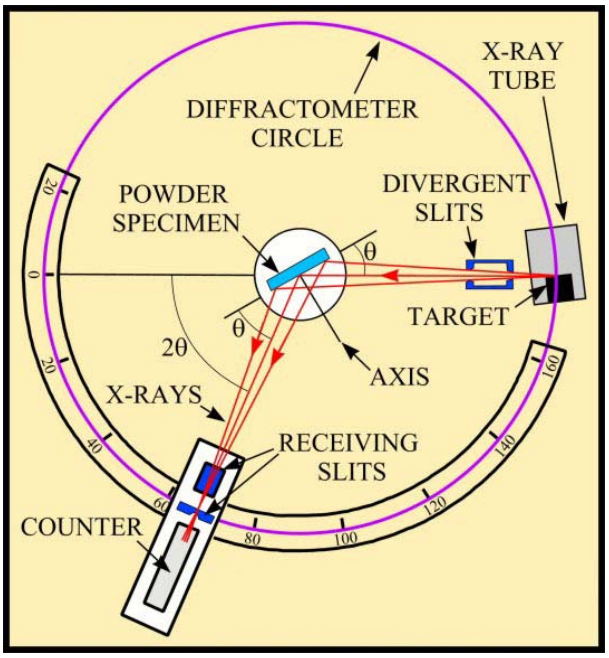

Figure 17 Diagram of a powder x-ray diffractometer
Source: Cullity (1956)

The x-ray spectrometer is shown in Figure 17. X-ray from the x-ray source is incident on a sample which is placed on a powder specimen. The diffracted x-ray passes through a slit to a detector. The sample is positioned so that its diffracting planes make some particular angle θ with the incident beam and the detector is set at the corresponding angle 2θ. The detector records the intensity of the diffracted beams and these can be plotted out as a function of 2θ. Each crystalline substance has its own characteristic powder diffraction pattern which may be used for its identification. Standard patterns are given in the powder diffraction file (known as the JCPDS file).

For standard $LaCoO_3$ JCPDF file No. 25-1060 shown in Figure 18, the characterization used Cu $K_{\alpha 1}$ as x-ray source, of which the wavelength is 1.540 Å.

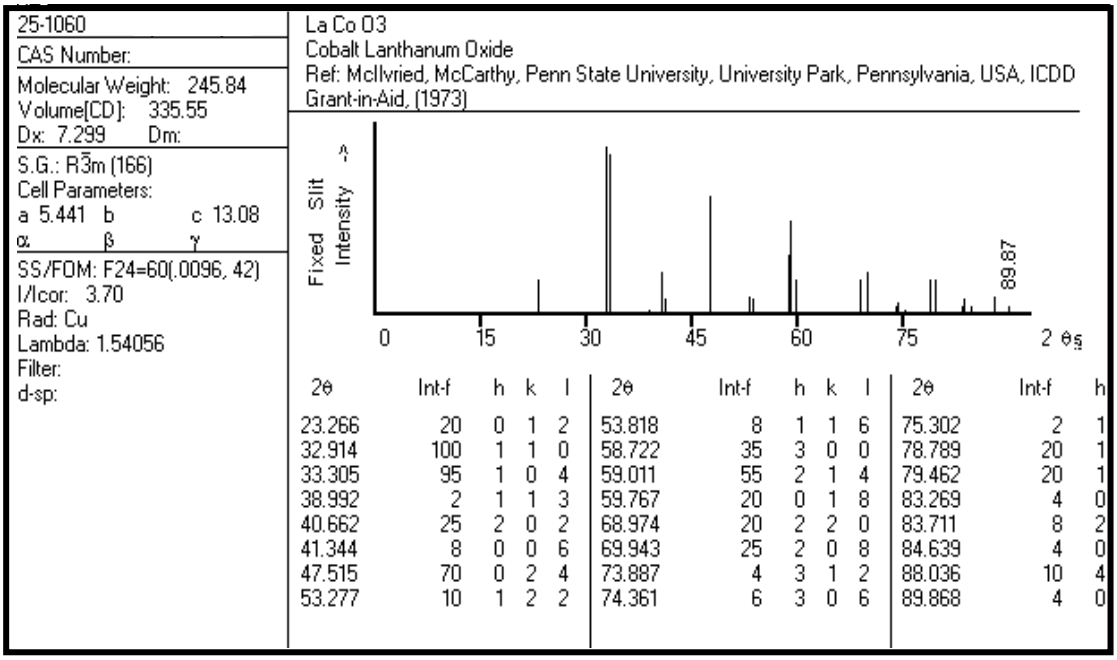

2θ	Int-f	h	k	l	2θ	Int-f	h	k	l	2θ	Int-f	h
23.266	20	0	1	2	53.818	8	1	1	6	75.302	2	1
32.914	100	1	1	0	58.722	35	3	0	0	78.789	20	1
33.305	95	1	0	4	59.011	55	2	1	4	79.462	20	1
38.992	2	1	1	3	59.767	20	0	1	8	83.269	4	0
40.662	25	2	0	2	68.974	20	2	2	0	83.711	8	2
41.344	8	0	0	6	69.943	25	2	0	8	84.639	4	0
47.515	70	0	2	4	73.887	4	3	1	2	88.036	10	4
53.277	10	1	2	2	74.361	6	3	0	6	89.868	4	0

Figure 18 Powder diffraction file (JCPDF) No. 25-1060 of $LaCoO_3$

Table 3 Unit cell parameters of crystal structure

Crystal system	Unit cell	formula	unit cell volume
Cubic	$\alpha = \beta = \gamma = 90°$ $a = b = c$	$\frac{1}{d^2} = \frac{h^2 + k^2 + l^2}{a^2}$	a^3
Tetragonal	$\alpha = \beta = \gamma = 90°$ $a = b \neq c$	$\frac{1}{d^2} = \frac{h^2 + k^2}{a^2} + \frac{l^2}{c^2}$	a^2c
Orthorhombic	$\alpha = \beta = \gamma = 90°$ $a \neq b \neq c$	$\frac{1}{d^2} = \frac{h^2}{a^2} + \frac{k^2}{b^2} + \frac{l^2}{c^2}$	abc
Hexagonal	$\alpha = \beta = 90°\ \gamma = 120°$ $a = b \neq c$	$\frac{1}{d^2} = \frac{4}{3}\left[\frac{h^2 + hk + k^2}{a^2}\right] + \frac{l^2}{c^2}$	$\frac{\sqrt{3}a^2c}{2}$

Source: West (1989)

Determination of crystallite size (Klung and Alexander, 1954)

Crystallite size can be obtained from XRD technique by measuring the diffraction line broadening. At the simplest level, the application of the Scherrer formula leads to an estimate of the mean crystallite size. The breadth of an x-ray reflection on the lattice planes of crystallites (small single crystals) depends upon the characteristics of the crystallites (size and defects in the lattice) and instrumental factors. Considering an x-ray reflection, Scherrer first showed that the mean dimension in micrometer, D, of the crystallites composing a powder is related to the pure x-ray diffraction broadening or the full width at half maximum intensity (FWHM) in radians, β, by the equation.

$$D = \frac{K\lambda}{\beta \cos\theta} \qquad .....(10)$$

where K is a constant

λ is the wavelength of the x-ray radiation employed

β is the full width at half maximum intensity (FWHM), often written as $\beta_{1/2}$, expressed in radians

θ is the angular position of the peak maximum.

The constant K depends upon the definitions of crystallite size and broadening, the shape of crystallites, and the reflection being examined. When $\beta_{1/2}$ is used, the value of K should be taken as 0.9.

The Schrerrer formula assumed that small crystallite size is the sole source of broadening of the diffraction profile. In fact, there is always a broadening due to the various instrumental factors such as slit widths, sample size, penetration of the x-ray beam into the specimen, imperfect focusing, or misalignment of the diffraction. By measuring experimental and reference lines, the true peak breadth which one use in equation (10) can be calculated by the Warren formula;

$$\beta^2 = \beta^2_{observed} - \beta^2_{reference} \qquad .....(11)$$

The applicability of line broadening analysis to catalysis is often restricted for a number of reasons. The reflections from the different solid phase might be superimposed. The other severe limitation comes from the lack of contrast between the intensity of reflection and that of overall scattering, particularly for metals with low atomic number such as Fe, Co, and Ni. Furthermore, there is also an upper limit of size beyond which crystallite size can no longer be measured because the broadening due to crystallite size becomes too small with respect to the instrumental broadening.

Single-phase crystallization of pure perovskite $LaMeO_3$ (Me = Mn, Co, Fe) phases were studied by Popa *et al.* (2002). $LaMnO_{3.15}$ had a rhombohedral symmetry after thermal treatment at 973 K (JCPDS 32-484), $LaCoO_3$ had a rhombohedral symmetry after thermal treatment at 923 K (JCPDS 25-1060) and $LaFeO_3$ had an orthorhombic symmetry after thermal treatment at 823 K (JCPDS 37-1493). Crystallite sizes of samples were calculated based on the FWHM of a diffraction peak using the Scherrer equation. Taguchi *et al*. (2002) prepared $LaCoO_3$ by citrate method. The crystallite sizes of $LaCoO_3$ synthesized at 873, 973, 1073 and 1173 K were 12.2, 16.4, 18.9 and 21.0 nm, respectively, which increased with increased synthetic temperature. Krupicka *et al.* (2002) studied the crystallite sizes of citrate precursors of $LaCoO_3$ calcined at 873 and 1073 K. The crystallite sizes were 9.7 – 10.7 nm and 13.5 – 15.4 nm, respectively. The $LaFeO_3$ perovskite was prepared by polymerizable citrate complex method. The average size under the calcination temperature of 873 K for 1 hour was about 40 nm (Zhao *et al.*, 2000).

2.3.2 X-ray Photoelectron Spectroscopy (XPS) (Niemantsverdriet, 1995)

X-ray Photoelectron Spectroscopy is among the most frequency used techniques in catalysis. It yields information on the element composition, the oxidation state of the elements and in favorable cases on the dispersion of one phase over another.

Photoelectron spectroscopy is based on the photoelectric effect. A sample that is irradiated with light of sufficient high energy greater than the energy holding the electron in the molecule can emit electron. When this technique has been used for surface studies it has been subdivided according to the source of exiting radiation into: (i) x-ray photoelectron spectroscopy (XPS) using soft x-ray (200-2000 eV) radiation to examine core-levels and (ii) ultraviolet photoelectron spectroscopy (UPS) using vacuum UV (10-45 eV) radiation to examine valence levels.

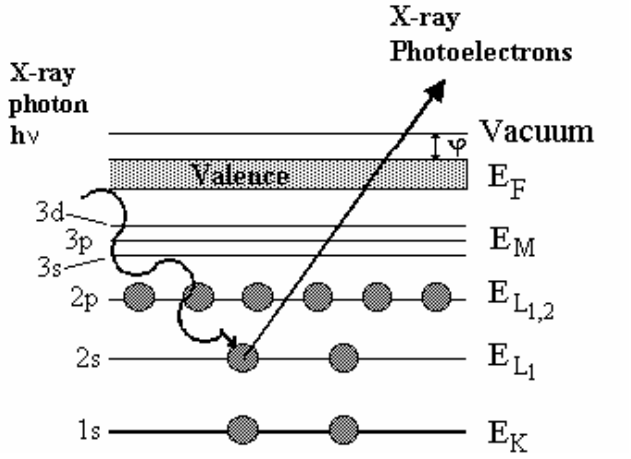

Figure 19 Photoionization process occurs in x-ray photoelectron spectroscopy
Source: Au (2004)

In x-ray photoelectron spectroscopy, when an atom absorbs a photon of energy hν, next a core electron with binding energy E_b is ejected with kinetic energy (Figure 19):

$$E_k = h\nu - E_b - \varphi \qquad .....(12)$$

where E_k is the kinetic energy of the photoelectron

h is Planck's constant

ν is the frequency of the exciting radiation

E_b is the binding energy of the photoelectron with respect to the Fermi level

φ is the work function of the spectrometer.

Measurement of its kinetic energy allows one to calculate the binding energy of the photoelectron. The atom stays behind as an unstable ion with a hole in one of the core level. By the Auger process (Figure 20), the atom relaxes by filling the hole via transition of an electron from an outer level. As a result of that transition the energy difference becomes available as excess kinetic energy, and this excess energy can be given to another electron either in the same level or in a more shallow level, whereupon the second electron, the Auger electron, is ejected.

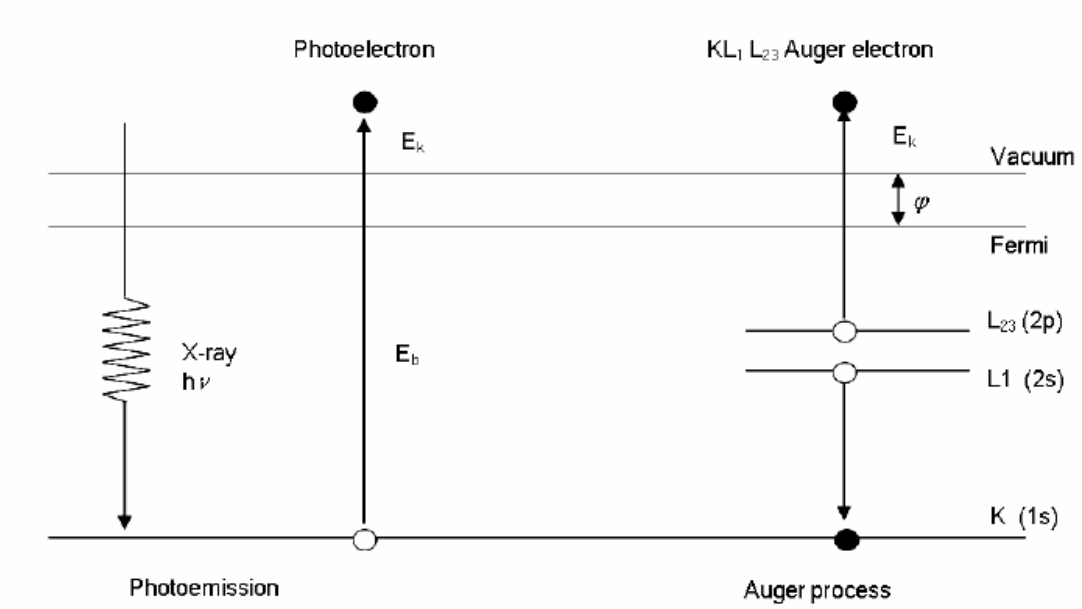

Figure 20 Photoionization process and Auger process
Source: Niemantsverdriet (1995)

The most commonly employed x-ray sources are Mg K_α (1253.6 eV) and Al K_α (1486.3 eV). XPS measures the intensity of photoelectrons N(E) as a function of their kinetic energy. The XPS spectrum, however, is usually a plot of N(E) versus E_k, or more often, versus the binding energy E_b.

XPS gives information on the elemental composition, the oxidation state of the elements and in favorable case on the dispersion of one phase over another. XPS are measured the intensity of photo electron N(E) as a function of their kinetic energy. The XPS spectrum is usually a plot of N(E) versus E_k or E_b. Photoelectron peaks are labeled according to the quantum number from which the electron

originates. An electron with orbital momentum l and spin momentum s has a total momentum j = l + s. As the spin may be up (s = +1/2) or down (s = -1/2), each level with l ≥ 1 has two sublevels, with an energy different called the spin-orbit splitting. Spin-orbit splitting as well as binding energies of particular electron level increase with increasing atomic number. Binding energy is not only element specific but contains chemical information as well, because the energy level of core electron depends slightly on the chemical of atom.

Figure 21 represents the general diagram of an XPS setup:

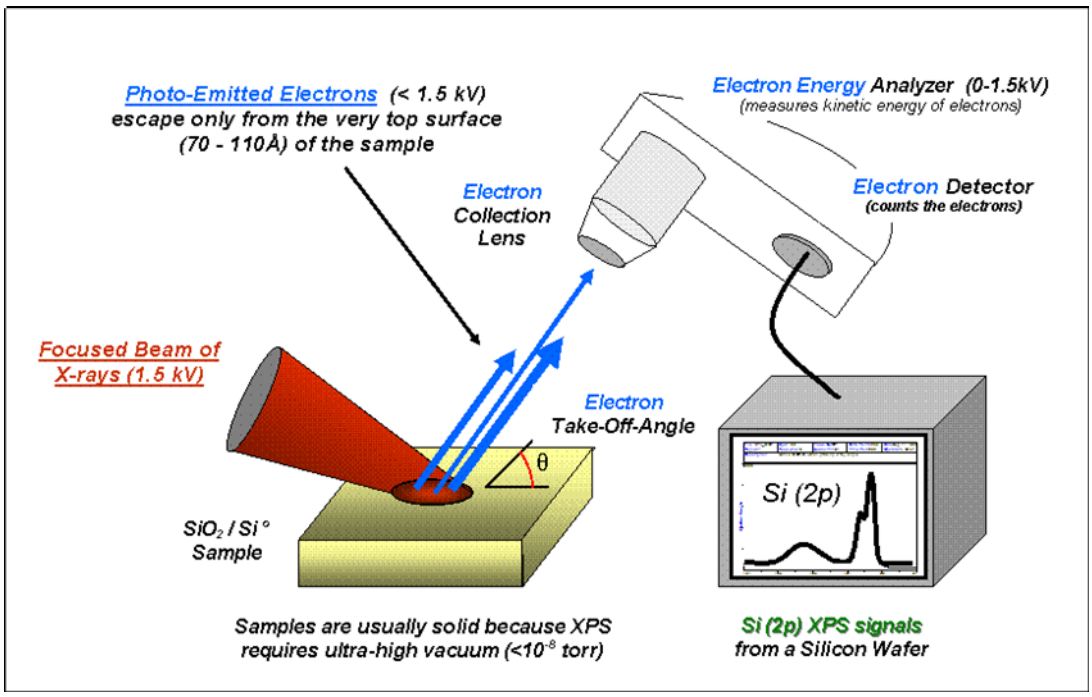

Figure 21 Basic components of a monochromatic XPS system
Source: Wikipedia (2007)

The analyzer (CHA - Concentric Hemispherical Analyzer), which allows a selection in energy of the photoelectrons, consists of two hemispherical electrodes. Shape of one hemisphere is concave, and the other convex. They are arranged such that their centers of curvature are coincident. Different voltages are placed on each hemisphere such that there is an electric field between the two hemispheres. Electrons are injected into the gap between the hemispheres. If the electrons are traveling very fast, they will

impinge on the outer hemisphere. If they are traveling very slow, they will be attracted to the inner hemisphere. The potential difference between these two electrodes defines the pass energy of the electrons. Only the electrons having a kinetic energy included in an interval of energy centered on this pass energy will arrive at the detector. At the end of the analyzer, a multiplying detector (channeltron) makes it possible to create secondary electrons.

The surface composition of $La_{0.95}Ce_{0.05}MnO_3$ perovskite calcined at 1073 K for 6 hours was studied by XPS (Zhang-Steenwinkel *et al.*, 2002). The resulting binding energy values were corrected using the C 1s peak at 285 eV. Two peaks of La $3d_{3/2}$ are located at 855.3 and 851.2 eV and those of La $3d_{5/2}$ are at 838.5 and 834.4 eV, respectively, with spin-orbit splitting 16.8 eV. Two peaks at 529.0 and 531.0 eV may be assigned to O 1s. Tan *et al.* (2002) prepared $LaCo_xMn_{1-x}O_3$ by the decomposition of the amorphous precursor $LaCo_xMn_{1-x}$ (DTPA).$6H_2O$ (x = 0.3 and 0.4) using $La(NO_3)_3$, $CoCl_2$, $MnCl_2$ and diethylenetriaminepentaacetic acid (H_5DTPA) as starting meterials. The binding energy of Co^{3+} was reported to be 779.5 eV and that of Mn^{3+} was 641.5 eV.

Examples of the XPS binding energy (BE) values of the references are presented in Table 4.

Table 4 XPS binding energy (BE) values of references

Sample	Binding energy (eV)					
	C1s	O1s	La $3d_{5/2}$	La $3d_{3/2}$	Co $2p_{3/2}$	Co $2p_{1/2}$
$La_{0.95}Ce_{0.05}MnO_3$[(a)]	285.0	529.0	834.4	851.2		
	286.5	531.0	838.5	855.3		
	289.2					
$LaCoO_3$[(b)]	284.8	529.2			779.8	795.0
		531.3				
$La_{0.8-x}Ce_xSr_{0.2}MnO_3$[(c)]	284.6	529.1	834.1	850.9		
		530.5				
		531.0				
La_2O_3[(c)]		529.0	834.2	851.0		
		531.0				
La-Co-O[(d)]	284.7	528.8-529.0	833.0		779.3	
		530.0-530.1				
		532.1-532.5				
$LaCoO_{3-\delta}$[(e)]	285.0				780.0	794.5
$LaCo_xMn_{1-x}O_3$[(f)]	284.7				779.5	
Co_3O_4[(f)]	284.7				779.8	

(a) Zhang-Steenwinkel (2002)
(b) Seim *et al.* (1997)
(c) Klyushnikov *et al.* (2002)
(d) Zhang *et al.* (2005)
(e) Muhakata (1997)
(f) Tan *et al.* (2002)

2.3.3 X-ray Fluorescence Spectroscopy (XRF) (Jenkins, 1999)

X-ray fluorescence spectroscopy can be used to measure all of the major elements composition in sample as well as a wide variety of trace elements.

When an atom is bombarded with x-ray photon, an inner orbital electron is ejected. The atom possesses vacancy in the inner shell. An outer orbital electron fills to the vacancy inner level and the excess energy following transference may be emitted as characteristic radiation. So the energy of the emitted x-ray photon is equal to the absolute energy difference between the binding energies of the initial and final state of the transferred electron.

Many atoms in the sample are changed in the excitation and all possible emission will be taken. It can be distinguished for the majority of observed wavelengths by simple selection rules. These are generally classified as three types:

(a) Normal transitions can be defined by a simple set of selection rules via $\Delta n \geq 1$, $\Delta l = \pm 1$ and $\Delta j = \pm 1$ or 0, where n, l and j denote the principle quantum number, angular momentum quantum number and spin-orbit coupling value respectively.

(b) Forbidden transitions do not obey the same set of selection rules.

(c) Satellite lines are wavelengths occurring from transitions following dual ionization of the atom. It explained that a second ionization occurs within the lifetime of the first excited state.

The transition of electron usually occurs following the normal transition. Moreover the forbidden and satellite transitions also occur but their intensities are usually low.

For each atom in the sample, the intensity of the characteristic x-ray will be proportional to the number of atoms in the sample. Thus the measured intensity of characteristic x-rays for each element can be compared to the intensity of known standard concentration, and determines the concentration of the element in the unknown.

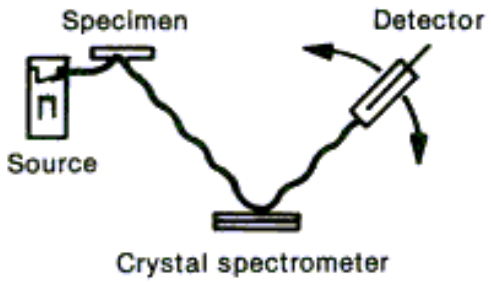

Figure 22 X-ray fluorescence spectrometer
Source: Jenkins (1999)

X-ray fluorescence spectrometer based on wavelength dispersive method Figure 22. It consists of an x-ray tube has a high voltage generator capable providing a potential of typically 40 to 100 kV and an anode of Cr, Rh, W, Ag, Au or Mo. It can produce x-rays capable of ejecting inner shell electron of all interested elements in the sample. The x-rays are produced in the sample and then sent through a collimator to produce a coherent beam.

The relationship between emission wavelengths and atomic number is known, isolation of individual characteristic line allows the unique identification of an element to be made and elemental concentrations can be evaluated from characteristic line intensities. Therefore, this technique can be used to determine the amount of element composition in the sample.

2.3.3 The Brunauer Emmett Teller method (Satterfield, 1980)

Adsorption measurements have a variety of uses and applications. The most important one is determining surface area of catalyst. The principle method of measuring total surface area of catalysts is by adsorption of a particular molecular species from gas or liquid onto the surface. If the condition under which a complete adsorption layer, averaging one molecule thick, can be established and the area covered per molecule is known, then the quantity of adsorbed material gives directly the total surface area of the catalysts.

The most common method of measuring surface area is calculated by the Brunauer, Emmett, and Teller (BET) equation in the form.

$$\frac{P}{V(P-P_o)} = \frac{1}{V_mC} + \frac{(C-1)P}{V_mCP_o} \quad .....(13)$$

where v = volume of gas adsorbed at pressure P.

v_m = volume of gas adsorbed in monolayer.

P_0 = saturation pressure of adsorbate gas at the experiment temperature

C = a constant related exponentially to the heats of adsorption and liquefaction of the gas

From the BET equation, a plot of $P/v(P_0-P)$ vs. P/P_0 should give a straight line whose slope and intercept can be used to evaluate v_m and C. Many adsorption data show very good agreement with the BET equation over values of the relative pressure P/P_0 between approximately 0.05 and 0.3, and this range is usually used for surface area measurements.

3. Catalytic Activity

According to various techniques mentioned, by using the appropriate combination of surface spectroscopies, the desired characterization on the atomic scale is certainly possible in favorable case. The disadvantage, however, is that although one may be able to study the catalytic properties of such samples under realistic conditions, most of the characterization is necessarily carried out under reaction condition. The approach that uses to study real catalysts either under reaction condition or, as it more often done, under a controlled environment after quenching the reaction is *in situ* techniques.

In situ Fourier Infrared transform spectroscopy (*in situ* FTIR) is one of the most powerful techniques used to monitor the catalytic reaction. Because infrared spectroscopy gives us the information about chemical bonding, *in situ* FTIR can be

use to identify the reactants and products in the reactions and study the kinetic of reaction as well. Infrared spectroscopy is the study of the interaction of infrared light with matter. When infrared radiation interacts with matter it can be absorbed, causing the chemical bonds in the material to vibrate. Due to the difference in bond strength, the energy corresponding to the vibration of each chemical bond becomes different causing one to identify functional groups which present in the matter. The most common application of infrared spectroscopy in catalysis is to identify adsorbed species and to study the way in which these species are chemisorbed on the surface of the catalyst. Among several modes of infrared spectroscopy used to characterize catalysts (Figure 23), diffuse reflectance mode is the most powerful form for measurement spectra of powder samples and this mode is called *in situ* diffuse reflectance infrared fourier transform spectroscopy (*in situ* DRIFTS).

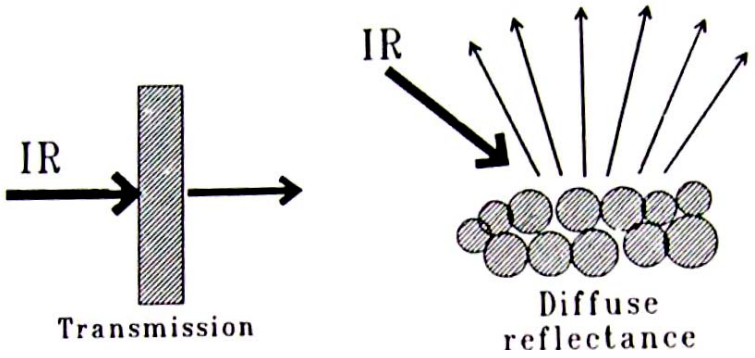

(a) (b)

Figure 23 Different forms of performing vibrational spectroscopy: a) transmission infrared on a wafer pressed from catalyst powder and b) diffuse reflectance infrared spectroscopy on catalyst powder

Source: Niemantsverdriet (1995)

Diffuse reflection spectroscopy (DRIFT) is the preferred infrared technique for studying organic coatings on inorganic powders. Using this technique infra-red radiation diffusely scattered from the surface of the sample is collected by a parabolic mirror and passed to a detector. Steps are taken to eliminate specular reflection. Functional groups present in the sample are identified from their characteristic absorption frequencies. The technique appears to have some surface specificity and

can detect surface species more easily than transmission spectra. A great advantage of infrared spectroscopy is that the technique can be used to study catalysis *in situ*.

When the IR beam enters the sample, it can either be reflected off the surface of a particle or be transmitted through a particle [Figure 24(a)]. The IR energy reflecting off the surface is typically lost. The IR beam that passes through a particle can either reflect off the next particle or be transmitted through the next particle. This transmission-reflectance event can occur many times in the sample, which increases the path length. Finally, such scattered IR energy is collected by a spherical mirror that is focused onto the detector [Figure 24(b)]. The detected IR light is partially absorbed by particles of the sample, bringing the sample information.

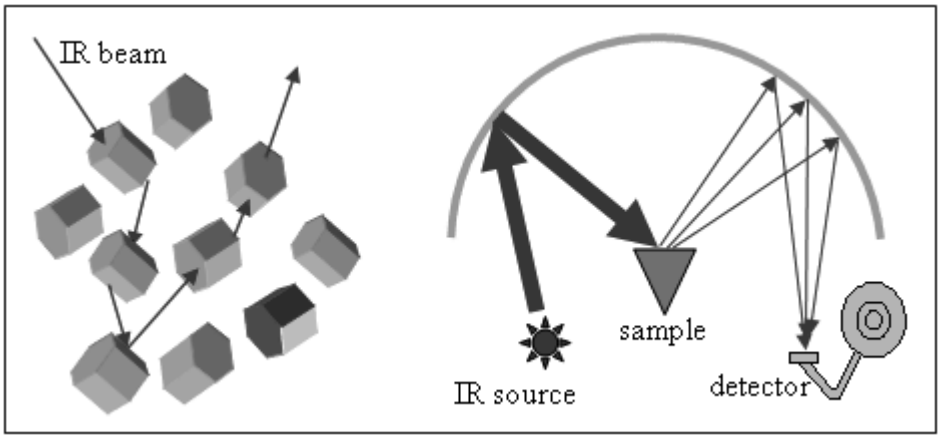

(a) (b)

Figure 24 (a) Mechanisms generating the infrared spectrum of a powder
(b) Ellipsoidal mirror used in the collection of diffuse radiation from the sample and focus them on the detector

Source: Keck-II (2006)

3.1 Catalytic oxidation of VOCs

Volatile organic compounds (VOCs) as for example aromatic and aliphatic hydrocarbon, alcohol, ketone and aldehydes of which catalytic combustion represents an effective tool for air pollution control. Several researchers have

investigated VOCs reactivity mainly on noble metal supported catalysts, showing a correlation between their oxidation rate and the bond dissociation energy of the weakest C-H bond. Transition metal perovskites i.e. $LaMO_3$ (M = Mn, Co) were known metal perovskites as oxidation catalysts and cheaper than noble metal supported catalysts (Spinicci *et al.*, 2003).

3.1.1 Oxidation of toluene

Alifani *et al*. (2005) studied the supported $LaCoO_3$ perovskites with 10 and 20 wt.% loading obtained by incipient wetness impregnation of $Ce_{1-x}Zr_xO_2$ supports with a citrate solution, prepared from La and Co nitrates, and citric acid. $Ce_{1-x}Zr_xO_2$ was also prepared using the citrate method. All materials were calcined at 973 K for 6 hours. These materials were tested for toluene total oxidation in the temperature range 373 – 773 K. The conversion of toluene was used as a primary measure of catalytic activity. Under the investigated conditions, CO_2 and water were the only detected reaction products. All catalysts showed a lower T_{50} (the temperature at which the conversion level of toluene is 50%) than the corresponding $Ce_{1-x}Zr_xO_2$ supports or pure $LaCoO_3$ perovskite. The activity of the catalysts was found to increase with the perovskite loading, irrespective of the support composition.

Supported $LaCoO_3$ perovskites with 10 wt.% loading were prepared by impregnation of different supports containing ceria with a solution of La and Co nitrates and citric acid (Alifani *et al*., 2006). All catalysts were tested for toluene total oxidation in the temperature range 373 – 873 K. $LaCoO_3$ is an active catalyst for toluene complete oxidation. Toluene total oxidation on perovskite-based systems is conducted to only non-noxious CO_2 without any CO or by-products formation. In spite of a large surface area, alumina-supported perovskites showed a lower global activity. It appears then the necessity of the presence of a perovskite phase for good oxidative activity. In terms of reaction rates higher reaction rates per perovskite weight were observed for all supported catalysts when compared to bulk $LaCoO_3$.

Li *et al.* (2004) investigated the catalytic combustion of toluene over Mn–containing mixed oxides. It was found that the catalytic activity gradually increased with an increase of Mn loading on ZrO_2. When Mn loading reached 50 mol%, the total conversion temperature was lowered to 533 K. Heat treatment of the catalysts led to the decrease in the activity of toluene conversion, however the toluene conversion remained still high, at 593 K after calcination up to 1023 K, which implied the catalyst was highly thermally stable.

Selective oxidation and dehydrogenation of benzyl alcohol have been carried out on $ABB'O_3$ (A = Ba, B = Pb, Ce, Ti and B' = Bi, Cu, Sb)-type perovskite oxides in the absence and in the presence of oxygen (Sumathi *et al.*, 1998). Partial reduction of the catalyst is observed when the reaction is carried out in the absence of oxygen or at low partial pressures of oxygen. Reduced catalysts were characterized by temperature-programmed reduction (TPR). TPR studies were carried out to determine the reducibility of the catalyst. Catalytic activity is found to depend on the reducibility of the catalysts. Copper-containing perovskites are highly reducible and $BaTiO_3$ and $BaCeO_3$ are the least reducible. Catalytic activity and reducibility are correlated with the metal-oxygen bonding as well as free energy of reduction of B site cations. The major products obtained in the partial oxidation of benzyl alcohol on all the perovskite oxides in the absence of oxygen are benzaldehyde and toluene. However, when the reaction is carried out in the presence of oxygen, small amounts of benzoic acid and benzyl benzoate are also obtained. In the absence of oxygen, hydrogen and water were also observed in the product stream. In the presence of oxygen in the reactant feed, however, no hydrogen was detected in the product stream.

3.1.2 Oxidation of propane

Merino *et al.* (2005) observed the activities of $La_{1-x}Ca_xCoO_3$ (x = 0, 0.2, 0.4, 0.5) perovskite-type oxides prepared by the citrate method. The reactivities of the different oxygen species were studied from the results of temperature-programmed desorption of oxygen and temperature-programmed

reduction. The catalytic behavior of $La_{1-x}Ca_xCoO_3$ (x = 0, 0.2, 0.4, 0.5) perovskites in the complete oxidation of propane was studied. Each data was the average of three steady-state measurements. The conversions at 533 K, the main products were CO_2 and water. On $La_{1-x}Ca_xCoO_3$, in the temperature range between 533 K and 573 K, traces of propylene and ethylene were detected. In the of $La_{1-x}Ca_xCoO_3$ an important increase in the propane conversion with the increase in the calcium amount was observed, especially for x = 0.4, where a conversion difference in the order of 20% at 533 K with respect to the unsubstituted perovskite was reached. The complete oxidation was reached at temperatures higher than 693 K for all of the catalysts except for $La_{0.5}Ca_{0.5}CoO_3$, for which total oxidation was reached at 673 K. The close parallel between the catalytic activity and the oxygen species amount adsorbed on the surface oxygen vacancies indicated that the propane oxidation on $La_{1-x}Ca_xCoO_3$ catalysts proceeds through a suprafacial reaction mechanism.

Barbero *et al*. (2006) investigated $La_{1-x}Ca_xFeO_3$ perovskite-type oxides with x = 0, 0.2 and 0.4 prepared by the citrate method. Catalytic performance was evaluated using propane. The main products during the total oxidation of propane were CO_2 and water. At reaction temperatures higher than 643 K, propylene was also detected and above 693 K, traces of CO and C_2H_4 were found. Other oxygenated products such as acrolein, acrylic acid, acetaldehyde were not found. The total oxidation of propane occurs through an intermediate, acetaldehyde. Propane oxidation starts at around 493 K. Considering the reaction temperature corresponding to 50% and 95% conversion of VOC (T_{50} and T_{95}), the activity for propane oxidation increases in the order: $La_{0.8}Ca_{0.2}FeO_3 < LaFeO_3 < La_{0.6}Ca_{0.4}FeO_3$.

3.1.3 Oxidation of ethanol

$La_{1-x}Ca_xFeO_3$ perovskite-type oxides with x = 0, 0.2 and 0.4 obtained by the citrate method were studied by Barbero *et al*. (2006). Catalytic performance was evaluated using ethanol. The main products during the total oxidation of ethanol were CO_2 and water. At reaction temperatures higher than 643 K, traces of CO and C_2H_4 were found. The total oxidation of ethanol occurs through an

intermediate, acetaldehyde. Considering the reaction temperature corresponding to 50% and 95% conversion of VOC (T_{50} and T_{95}), the activity for ethanol oxidation increased with increasing x.